FAILURE CRITERIA
FOR VISCOELASTIC MATERIALS

W. G. Knauss

GALCIT-SM-67-2 MARCH 1967

Semi-Annual Status Report

1 July 1966 - 28 February 1967

National Aeronautics and Space Administration
Research Grant No. NsG-172-60
GALCIT 120

Firestone Flight Sciences Laboratory
Graduate Aeronautical Laboratories
California Institute of Technology
Pasadena, California

INTRODUCTION

This semi-annual report reviews the results obtained since 1 July 1966 under the research grant NsG-172-60, GALCIT 120. Work under this grant has been concerned with several problems relating to fracture in viscoelastic materials which are listed in the order in which they will be discussed below.

I Material Characterization
- a) linear viscoelastic materials
- b) non-linear viscoelastic response
- c) non-linear response in the swollen state

II Stress Analysis of Crack Geometries Under Large Deformations
- a) experimental evaluation
- b) incremental solution for a linearly elastic material
- c) incremental computer solution for a non-linearly elastic material

III Comparison of Theory and Experiment for Failure Under Uniaxial Cyclic Strain

IV Crack Propagation in a Strip
- a) theoretical work
- b) experimental determination

Items I and II are necessary prerequisites to a refined failure analysis such as embodied in items III and IV. The latter two areas of investigation develop methods to better understand the failure process under varying stress or strain histories in viscoelastic materials.

I MATERIAL CHARACTERIZATION

The linear behavior of viscoelastic materials is well understood on a phenomenological basis. In using the viscoelastic material functions for calculations in stress analysis it is often necessary to know, interchangeably, the relaxation modulus, the creep compliance and the complex modulus and compliance. The latter two forms are necessary when dealing with cyclic load histories such as in the failure growth under cyclic strain.

a) Linear Viscoelastic Materials. Although failure is usually associated with large deformations, it has been found repeatedly that (modified) linear viscoelastic analysis has provided quantitative answers to fracture problems. In order to minimize the amount of experimental work in determining the various material properties, it is desirable to interconvert one material function into the other. Approximate methods to do this have been available for some time.

One particularly attractive way is the use of prony series representation. However, simple collocation techniques are not satisfactory for many applications and a more accurate method for determining the prony coefficients is needed. This can be achieved if the relaxation spectrum is known. Since from the polymer science point of view characterization of a material by the relaxation spectrum is much more informative than say the relaxation modulus, an investigation was therefore started some time ago to calculate numerically the relaxation spectrum and to compile a set of computer programs which would automatically calculate the relevant material function from one function (say relaxation or dynamic modulus) by way of the relaxation spectrum. This investigation is now in the final stage. The key findings are that the numerical solution of the integral equation

$$E_{rel}(t) - E_R = \int_0^\infty H(\tau)\ e^{-t/\tau}\ \frac{d\tau}{\tau} \qquad (1)$$

for $H(\tau)$ is not a straightforward matter which can be achieved economically with great accuracy. In order to determine the accuracy of the procedure, a special function $H(\tau)$ was chosen as the modified power law

$$H(\tau) = \frac{E_{rel}(o) - E_R}{\sqrt{\pi\tau}} \exp\left[-\frac{1}{\tau}\right] \tag{2}$$

from which the relaxation modulus is determined as

$$E_{rel} = E_R + \frac{E_{rel}(o) - E_R}{(1+t)^{\frac{1}{2}}} . \tag{3}$$

Using this expression for E_{rel} as input to the numerical program one can now calculate from (1) $H(\tau)$ and compare it with (2). In order to compare some standard approximate methods with the numerical scheme, two approximations of the Widder-Post type are shown in figure 1 through 3. Each figure shows the limitation of the separate methods from a different viewpoint. The numerical method gives results which oscillate about the exact one while the approximate methods deviate consistently from the exact solution, though less than the maximum variations of the digital computer calculations. It is important to note, however, that on the basis of figure 3 the average error of the numerical scheme is approximately zero whereas the Widder-Post results lead to a net non-zero error.

In applying the same technique to the determination of the retardation spectrum $L(t)$ certain difficulties arose. The creep compliance is given by

$$\begin{aligned} D_{creep} &= D_{creep}(o) + \int_o^\infty L(\tau)\left[1 - e^{-t/\tau}\right]\frac{d\tau}{\tau} \\ &= D_{creep}(o) + \int_o^\infty L(\tau)\frac{d\tau}{\tau} - \int_o^\infty L(\tau)\, e^{-t/\tau}\frac{d\tau}{\tau} \\ &= D_{creep}(\infty) - \int_o^\infty L(\tau)\, e^{-t/\tau}\frac{d\tau}{\tau} \end{aligned} \tag{4}$$

The form

$$D_{creep}(\infty) - D_{creep}(1) = \int_0^\infty L(\tau)\ e^{-t/\tau}\ \frac{d\tau}{\tau} \qquad (5)$$

is of the type of equation (1). Therefore, the same numerical computer program was applied to this equation. The results for $L(\tau)$ were inexplicably unreasonable in the sense that $L(\tau)$ was not a monotonic function as it should be. Because the computer program worked well for equation (1) the unreasonable behavior of the retardation spectrums is likely to be the result of the pecularities of the integral equation (about the numerical solution of which little is known) and the sensitivity of the solution to the type of function to be determined [$H(\tau)$ or $L(\tau)$][+]. It is evident from figures 1 through 3 that the approximate methods of the Widder-Post type give results which are generally as good as or better than the numerical calculations. It should be borne in mind, however, that this is at least in part due to the fact that the relaxation modulus is known as an analytic function. In a practical case that function would be known only as numerical data and the determination of the relaxation spectrum would involve determining first and second derivatives graphically which is not an accurate process. It appears, therefore, that the numerical method would, in general, yield quite acceptable results which can be used to convert relaxation data into creep and dynamic viscoelastic properties.

b) Non-linear viscoelastic response. Over the past year some effort has been directed to examining the viscoelastic behavior of Solithane 113 under large strains. Attempts to fit experimental data into existing theories have not been successful to date. One primary reason is that the data does not seem to follow a simple pattern. Figure 4 illustrates this deficiency most clearly; it gives the results of relaxation

[+] The essential difference between $H(\tau)$ and $L(\tau)$ is that $H(\tau)$ rises fast with τ and decreases slowly with τ after the maximum is reached, while $L(\tau)$ rises slowly with τ and drops to zero fast after the maximum.

tests in which the strain was increased in steps at the given temperature and then held constant. Although a new ring specimen was used at each temperature, the behavior at 60 per cent strain soon deviates from that at other strains as the temperature is lowered and as the temperature approaches the glass transition temperature this anomalous behavior shifts to higher strains (-17.5°C) and vanishes again as the glass transition is passed.

c) Non-linear Response in the Swollen State. The swelling of rubberlike materials has been used in order to quickly obtain an equilibrium position in the case of stress-strain measurements. Part of the internal viscosity of the material is taken out by swelling it in a suitable agent. Swelling also affects the constant C_2 in the standard Mooney-Rivlin stress-strain law, it reduces C_2 and tends to make the material more Neo-Hookean.

In order to reduce the complexity of a study of the fracture process in Solithane by decreasing the internal viscosity, the material characterization in the swollen state was undertaken as a first step in this direction.

The solubility parameter δ of Solithane 50/50 in a poorly hydrogen bonded solvent was experimentally determined to be $\delta = 9.6 \sqrt{\text{cal/cm}^3}$. This result led to the selection of Toluene ($\delta = 8.9$) as a swelling agent. Toluene swelling increases the volume of Solithane by 145%, i.e. the linear increase is 35%. Rough checks of the sol-fraction in Solithane 50/50 showed it to be less than 1 weight per cent.

Stress-strain tests were now performed at different strain rates and temperatures with the tensile specimen completely submerged in Toluene during the full length of the test. A tank-type apparatus, which can be inserted into the Instron testing machine, was especially designed for that purpose. The specimens had a dogbone shape.

The tests were run at strain-rates ranging from 0.00725 in./in.min. to 7.25 in./in.min. and temperatures ranging from 5°C to 40°C. Very good agreement of the stress-strain data with the behavior predicted by the classical theory of rubber elasticity was found at all rates and temperatures. The experimental error was in the order of $\pm 3\%$. Figures 5, 6, and 7 show the data in form of Mooney-Rivlin plots for several strain rates and

temperatures. Note that the stress changes with temperature in the manner predicted by classical rubber elasticity theory, i. e., the stress is proportional to T. These results yield the constant $\overline{C}_1 = C_1/T$ in the equation $\sigma = 2\overline{C}_1 T [\alpha - \alpha^{-2}]$ to be $\overline{C}_1 = 0.525$ psi/^{o}K, where stress and extension ratios are based on the dimensions of the swollen unstretched sample. Using this constant, which corresponds to a Youngs modulus of E = 465 psi for small extension ratios at room temperature, the effective number of chains was calculated to be 5.89×10^{-4} moles/ml. This corresponds to a sol-fraction of 0.6 weight per cent and a tensile modulus of ~500 psi according to the measurements of L. Smith and A. M. Magnusson.[+]

Assuming the sol-fraction to be zero, the polymer solvent interaction parameter μ was calculated from the equation given by Bueche and Dudek[++], it turned out to be $\mu = 0.492$.

In conclusion it can be said that the Solithane 50/50-volume composition swollen in Toluene yields a material behavior which conforms very well with the results given by the classical theory of rubber elasticity and has largely reduced internal viscosity as far as the stress-strain behavior is concerned. This material behavior should facilitate a study of the fracture process which is expected to contribute to the further understanding of this difficult problem.

[+] L. L. Smith and A. M. Magnusson; Journal of Polymer Science, 42, 391, (1960).

[++] T. J. Dudek, and F. Bueche; Rubber Chemistry and Technology, 37, 894, (1964).

II STRESS ANALYSIS OF CRACK GEOMETRIES UNDER LARGE DEFORMATIONS

As mentioned under the previous section, failure in polymeric materials is usually associated with large deformations. In the event that one wishes to study failure as a process of crack propagation, one must know the deformations and stresses at the tip of the crack. The development of this knowledge has been divided into three parts which are discussed subsequently.

a) Experimental Evaluations: Earlier experimental results had indicated that linear elastic theory could be used with some modification to approximately predict stresses and deformations under surprisingly large deformations. There remained the question, however, whether these measurements included tearing at the crack tip or not. Experiments with sheets of natural rubber have now been conducted to show that tearing does not occur until rather large strains are applied (for definition of terms for the tests see figure 3). The first tearing was observed at a gross strain of approximately 40 per cent. The question that arises now is, of course, why the material should withstand such high strains before rupturing. One obvious answer is that natural rubber crystalizes under strain and can thus withstand larger strains than other materials. There is one other explanation, which heretofore has been recognized as a possibility but which has eluded quantative evaluation: the strain alleviating effect of large deformations. This is discussed in the next part.

b) Incremental solution for a linearly elastic material. Solutions of problems in classical elasticity are essentially valid if the strains are infinitesimal everywhere in the stressed body. The solution, say the stress τ, depends on the applied load P in a linear fashion

$$\tau \sim P$$

If there are stress risers in the body, then linear solutions are valid as long as the material behaves in a linear fashion and the boundaries do not move significantly so as to allow satisfaction of the boundary conditions in a simple form. At any rate we can write a differential solution which is always valid

$$d\sigma = K(P)\ dP \qquad (6)$$

where K is a function of the load P through the deformed state of the body. If this equation is integrated, one obtains a solution which allows for large deformations provided the material behaves always linearly elastically. The latter condition is well approximated by rubbers under moderate strains. In this manner the problem of an infinite sheet containing an elliptic perforation was solved. The strain and strain concentration factor at the root of the ellipse are shown in figures 9 and 10, respectively, as a function of the applied gross strain. Whereas classical, linear elasticity predicts constant strain concentration factors (corresponding to those at zero strain) the present treatment leads to marked reduction with gross strain and thus to markedly lower strain values at the ellipse root than linear theory would predict. Because the material is assumed to be hookean, the reduction in strain is due entirely to kinematic effects under large deformations. The stress concentration factor is equal to the strain concentration factor.

c) Incremental computer solution for a non-linearly elastic material. In order to incorporate the non-linear material properties into the analysis it was necessary to write a computer program. Following essentially the incremental procedure in the previous discussion the load is applied in small but finite increments. Preliminary results are shown in figure 11. As for the incremental linear analysis, the stress and strain concentration factors decrease in the same characteristic fashion with the applied strain. But due to the non-linear material properties (neo-hookean material) the concentration factors decrease fast with applied strain and they are no longer equal. Work along these lines is continuing.

III COMPARISON OF THEORY AND EXPERIMENT FOR FAILURE UNDER UNIAXIAL CYCLIC STRAIN

In the last semi-annual report[+] calculations were presented which indicated the effect of maximum strain and frequency in a cyclic uniaxial strain experiment on the failure time. Using these calculations as a guide, experimental work is underway to examine this validity.

Two points have become clear from the experimental work. The qualitative behavior is as predicted by the calculations, but results are too sparse to derive more definite conclusions at this time. The limitation has been in the equipment which allowed use of only a single frequency and strain amplitude. The second point of interest is, that depending on the frequency and/or temperature the ring specimens follow a physically reasonable but seldomly considered or reported loading cycle. Upon unloading, the viscoelastic ring cannot contract as fast as the strain-producing ram, thus leaving the material free to contract under zero load for part of the cycle. The deformation history is thus prescribed by a given strain history during part of the cycle, the remainder of the cycle having zero stress specified; the history can be written as

$$\begin{aligned} \epsilon(t) &= \sin \omega t && 0 \leq t < t^* \\ \sigma(t) &= 0 && t^* \leq t \leq \frac{2\pi}{\omega} \end{aligned} \tag{7}$$

[+] Failure Criteria for Viscoelastic Materials, California Institute of Technology, Pasadena, California, GALCIT SM 66-10, June 1966.

which is given graphically in figure 12 below.

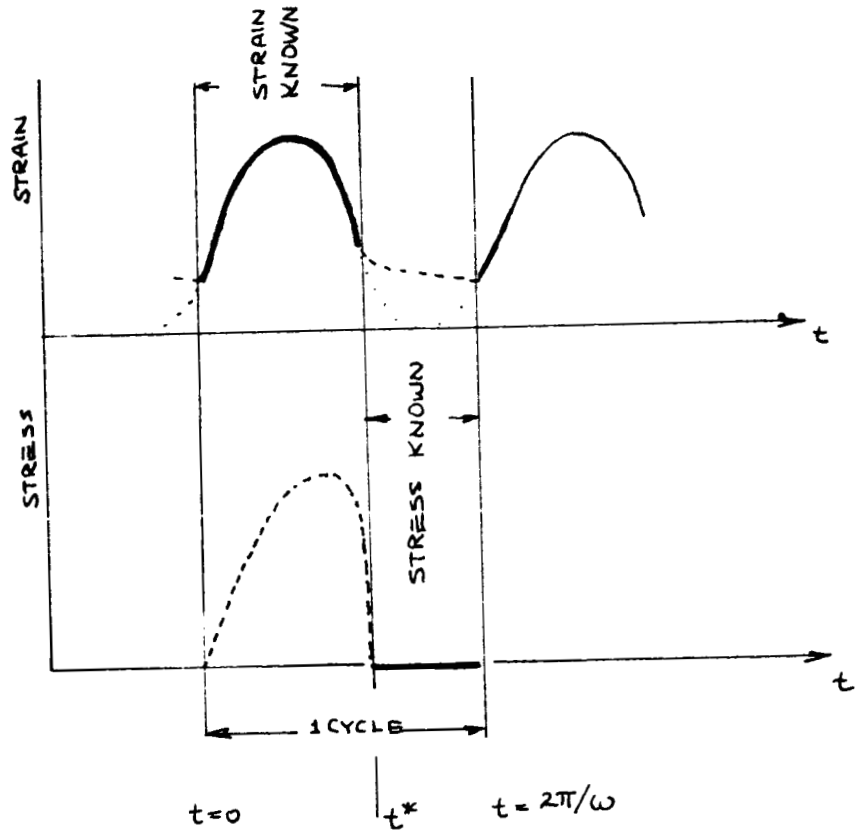

Figure 12. Load History On Ring Specimen Under Cyclic Extension At Relatively High Frequencies

The deformation and stress during each cycle are dependent on these split conditions. The determination of the stress and strain history requires the solution of a Fredholm integral equation of the first kind

$$\phi(t^*) + \int_0^{t^*} \frac{\frac{\partial}{\partial t^*} K^*(\tau, t^*)}{K^*(t^*, t^*)} \phi(\tau)\, d\tau + \varphi'(t^*) = 0 \qquad (8)$$

where t^* is also a function of the frequency. This type of loading history has not been considered heretofore. At present we restrict ourselves to load histories in which the strain is always known (and the stress therefore also; $t^* = \frac{2\pi}{\omega}$) which restricts experimental work to relatively low (temperature reduced) frequencies.

Figure 13 shows the typical plot of the failure time in a cyclic strain experiment as a function of temperature. At the test frequency (1.2 sec/cycle) the strain history was sinusoidal above 12°C and of the discontinuous type (illustrated in figure 12) below that temperature. Accordingly one should differentiate between the time to failure from the beginning of the test (accured failure time) and the total time the specimen was under stress. Figure 14 shows the failure time as a function of the maximum observed stress. It is clear from both figures 13 and 14 that the time to failure passes through a minimum as a function of applied load, temperature or frequency.

IV CRACK PROPAGATION IN A STRIP

In order to better understand the basic processes involved in fracture, the growth of a crack in a strip has been studied under various load histories. The work may be divided into two areas, one being theoretical, the other experimental.

a) Theoretical Work. For a crack propagating in a viscoelastic medium, the strain energy released by the system is transformed not only to surface free energy, but also into dissipation and kinetic energy. Thus, the Griffith energy equation for the growth of a crack in an elastic material is

$$\frac{\partial}{\partial t} [W-F-2D-K] = 0 \tag{9}$$

where W is the total input work, F is the Helmholtz free energy of the system, D is the total dissipation due to heat loss and K, the kinetic energy.

If we consider a crack propagating with a constant velocity, the rate of change of kinetic energy is zero. In the energy balance equation the evaluation of W and F is the same as for the elastic material. To calculate the rate of change of dissipation we assume that the stress field for a slowly moving crack is the same as that of a stationary crack, furthermore, assume that the dissipation is only effected by the stress concentration field. Accordingly, the expression of the rate of dissipation for a viscoelastic material can be derived from the fundamental definition. The analytical expression of the rate of dissipation seems very difficult to obtain due to the complexity of the integration process involved. However, it can be found numerically for discrete points in the domain of interest. The rate-of-dissipation density at the crack tip was found unbounded while the total rate of dissipation for a finite domain around the crack tip has been shown to be bounded. This fact will enable us to extend the Griffith type energy balance to the growth of cracks in viscoelastic materials. A computer program is under way to accomplish the numerical integration.

In the calculation process special care must be taken due to the presence of improper integrals which need to be evaluated analytically before numerical integration can be accomplished.

b) Experimental Work. Crack propagation in monotonic strain histories has been studied previously; to round out the experimental evaluation, tests are in progress for cyclic strains.

The major difficulty has been the recording of the crack advancement which must be accomplished with kinematographic means. In order to cover a sufficient range of crack velocities, it was necessary to develop lighting and film developing techniques for the particular experimental set up available in our laboratories. The methods developed give now satisfactory results. Since the film records give the crack position as a function of time, the velocity must be obtained by numerical differentiation. A typical plot of the crack velocity compared to the applied strain is given in figure 15. The important observations are: The shape of the velocity-time trace is different from the shape of the applied strain-time trace. This fact is simply the result of the non-linear relation between the applied strain and the crack velocity. Although this is clear on physical grounds, this fact has not always been appreciated in proposed failure calculations. A fact appreciated even less is that the velocity cycle lags behind the strain cycle. This is clearly the effect of viscoelastic material response. It is interesting to note, however, that the lag appears larger than one would expect on the basis of simple viscoelastic behavior at these temperatures ($20^{\circ}C$) and cycle rates (6 cycles per second). In order to quantitatively evaluate this behavior for a more definite physical interpretation, it is necessary to obtain more test data than have been obtained to date. Data reduction by current hand calculation methods is slow and inaccurate. Therefore, existing equipment is currently being modified to reduce the film records semi-automatically onto IBM cards which can then be used in conjunction with a Fourier analysis to obtain velocity plots (and then phase lag between maximum strain and maximum velocity) simply and in a straightforward way. Card punch equipment and digitizer circuits are already available and film reading equipment only needs modification to allow for simultaneous reading of the time scale and the crack position through a switching unit. The latter is under construction.

CONCLUSION

In summary we can state that apparently insurmountable problems exist only with respect to the concrete behavior of Solithane 113* under large strains. Further work will emphasize consolidation and amplification of the results reported here rather than the opening of new problem areas.

---

* Because this material is being made controllably in our laboratory and because it can fracture under small strains where linear viscoelastic behavior may suffice for characterization, we plan to continue using this material rather than starting with another one.

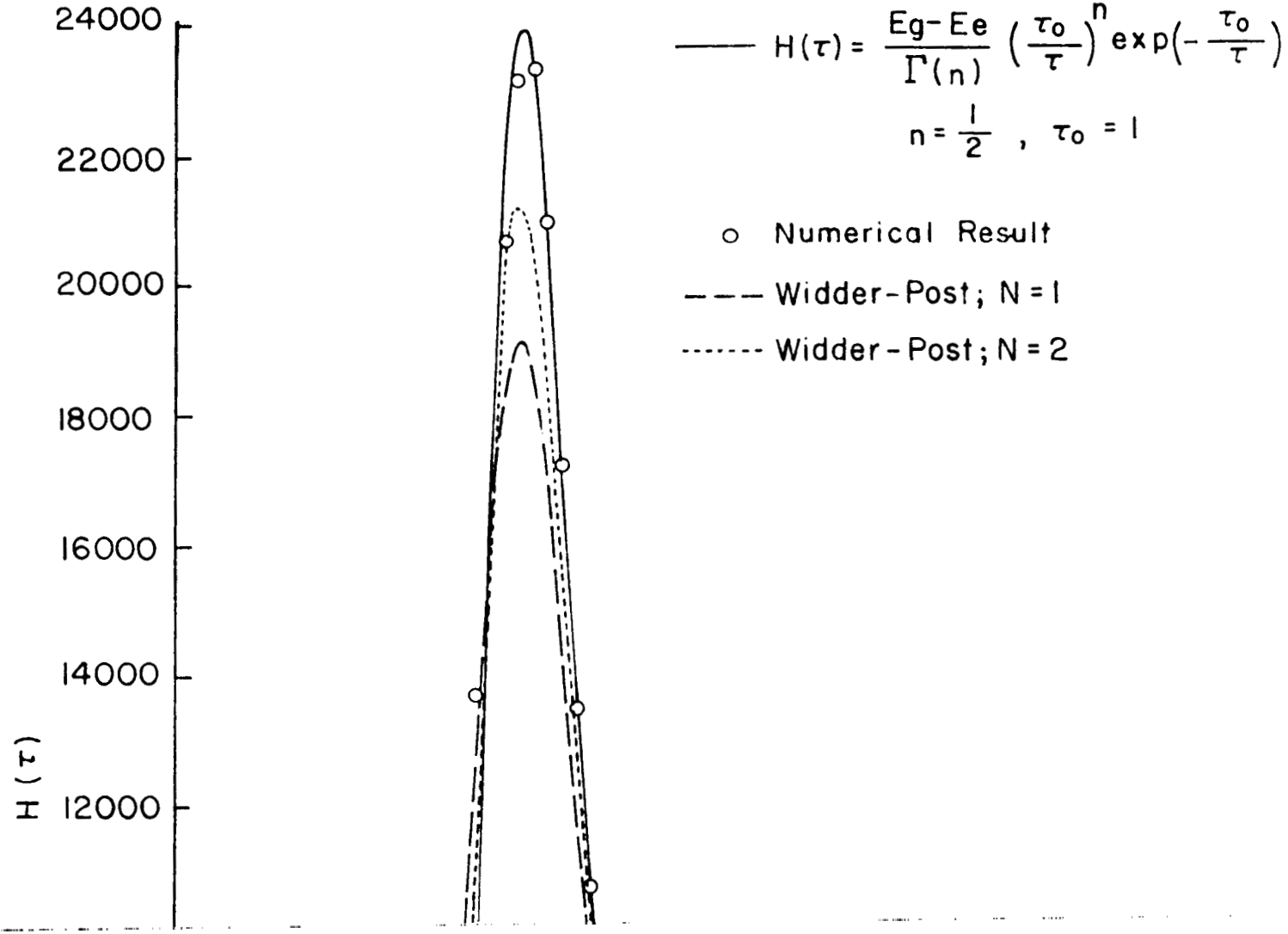
24000
22000
20000
18000
16000
14000
12000
H(τ)
$H(\tau) = \frac{Eg-Ee}{\Gamma(n)} \left(\frac{\tau_0}{\tau}\right)^n \exp\left(-\frac{\tau_0}{\tau}\right)$
$n = \frac{1}{2}$, $\tau_0 = 1$
Numerical Result
Widder-Post; N = 1
Widder-Post; N = 2

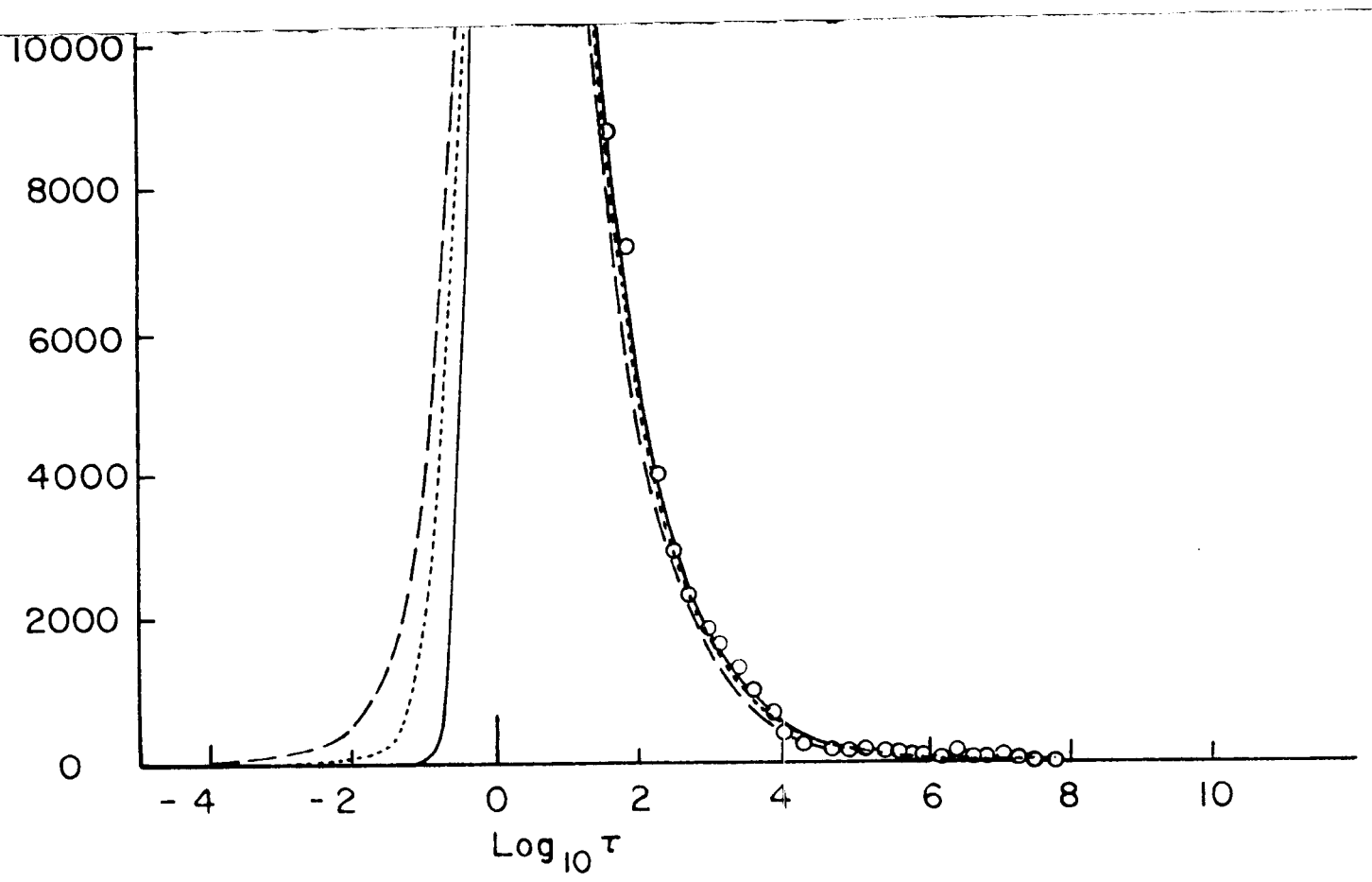

FIG. 1 COMPARISON OF EXACT, NUMERICAL, AND APPROXIMATE RELAXATION SPECTRA

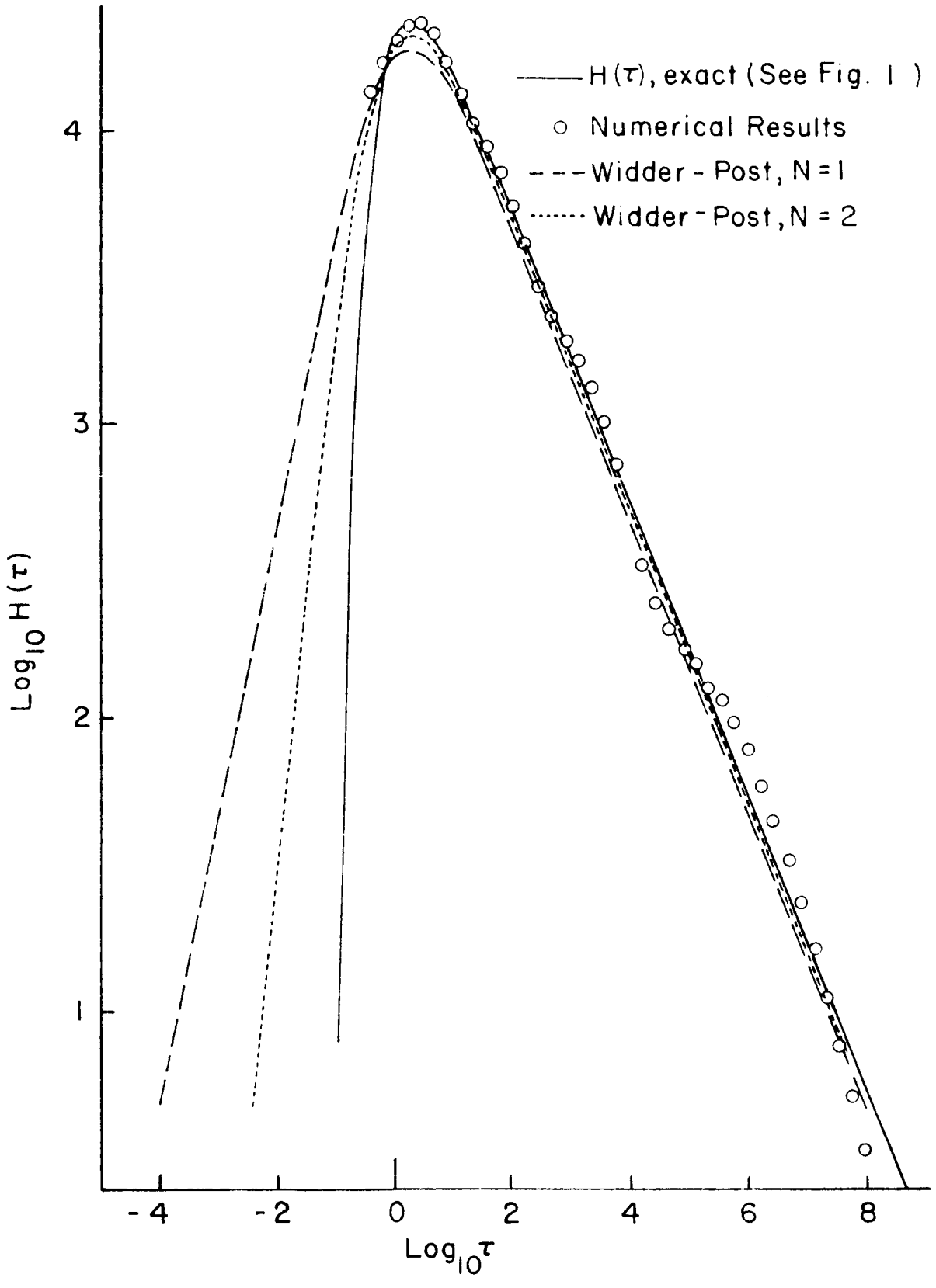

FIG. 2 LOGARITHMIC COMPARISON OF EXACT, NUMERICAL, AND APPROXIMATE RELAXATION SPECTRA

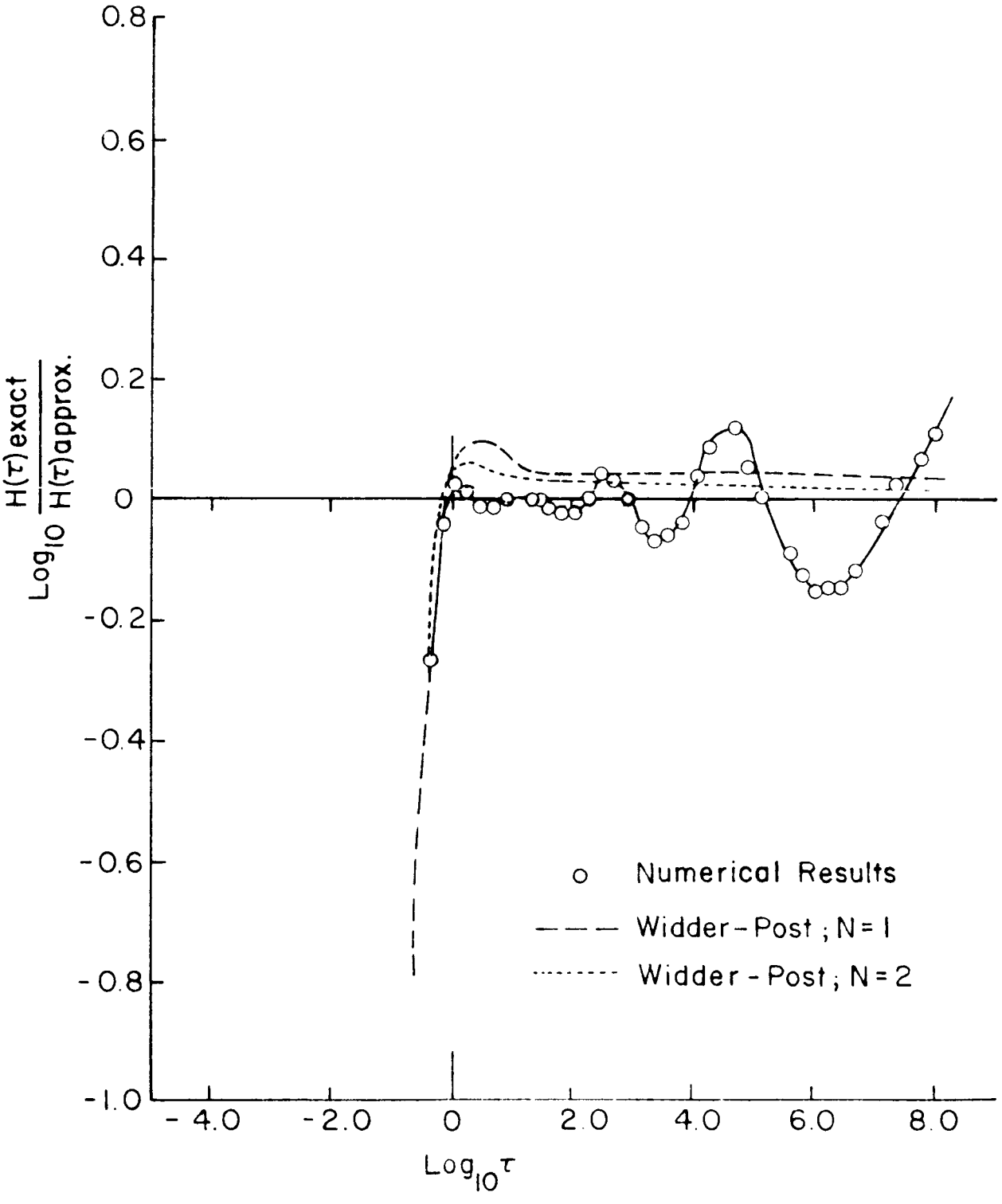

FIG. 3 ERROR IN RELAXATION SPECTRUM AS DETERMINED NUMERICALLY AND BY THE WIDDER-POST METHOD

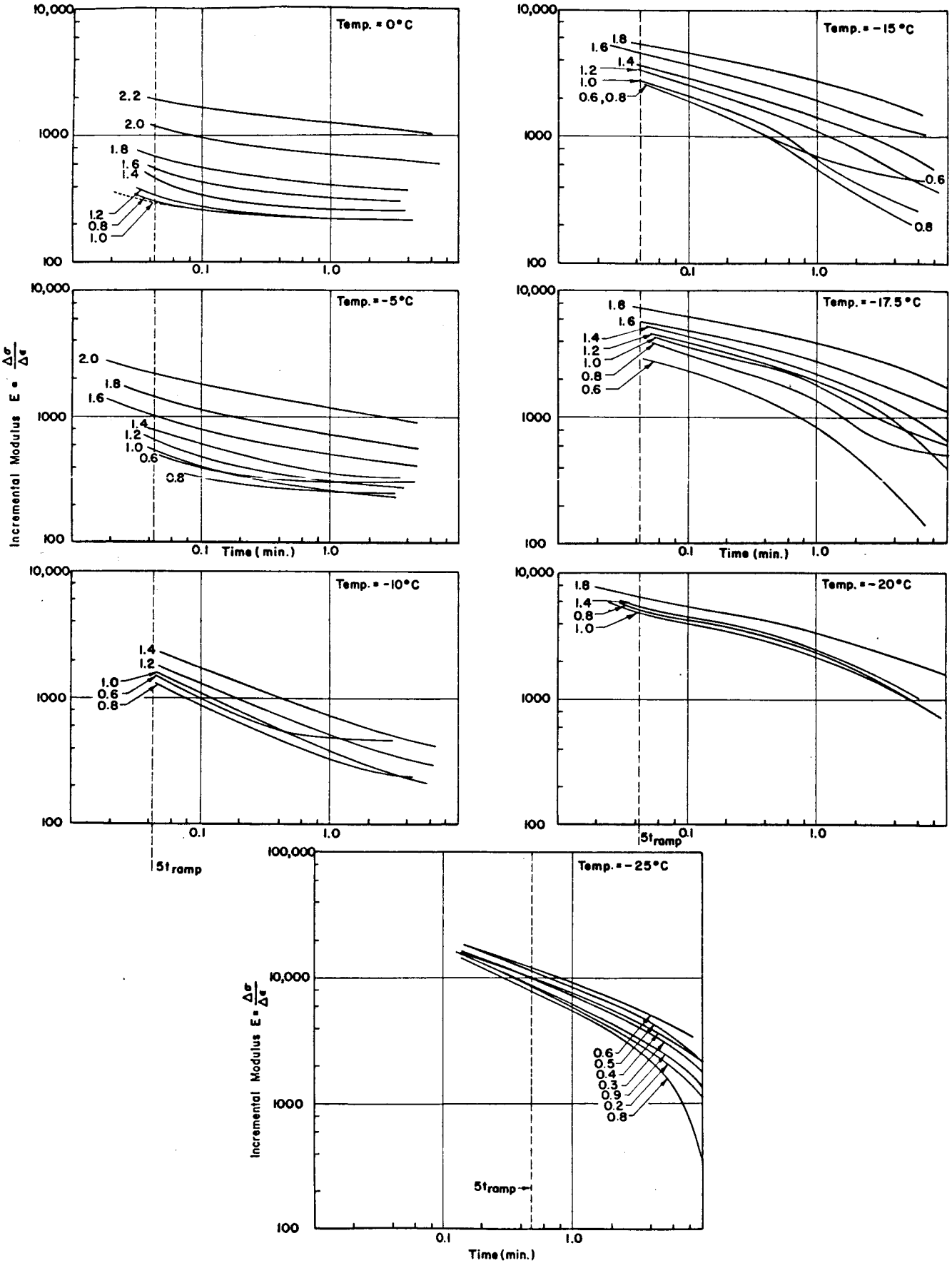

FIG. 4 INCREMENTAL RELAXATION MODULUS

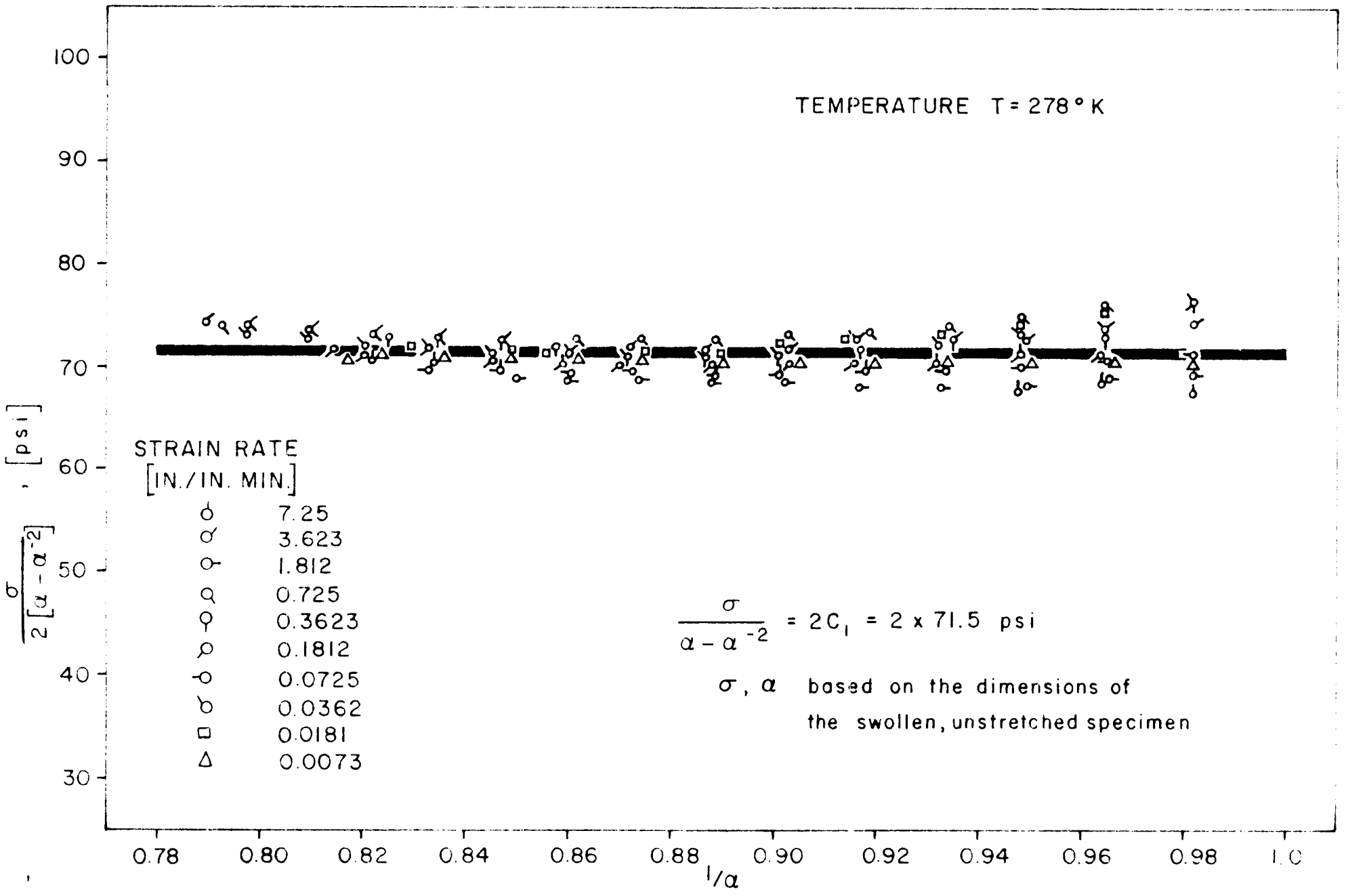

FIG. 5 MOONEY-RIVLIN PLOT FOR SOLITHANE 50/50 SWOLLEN IN TOLUENE

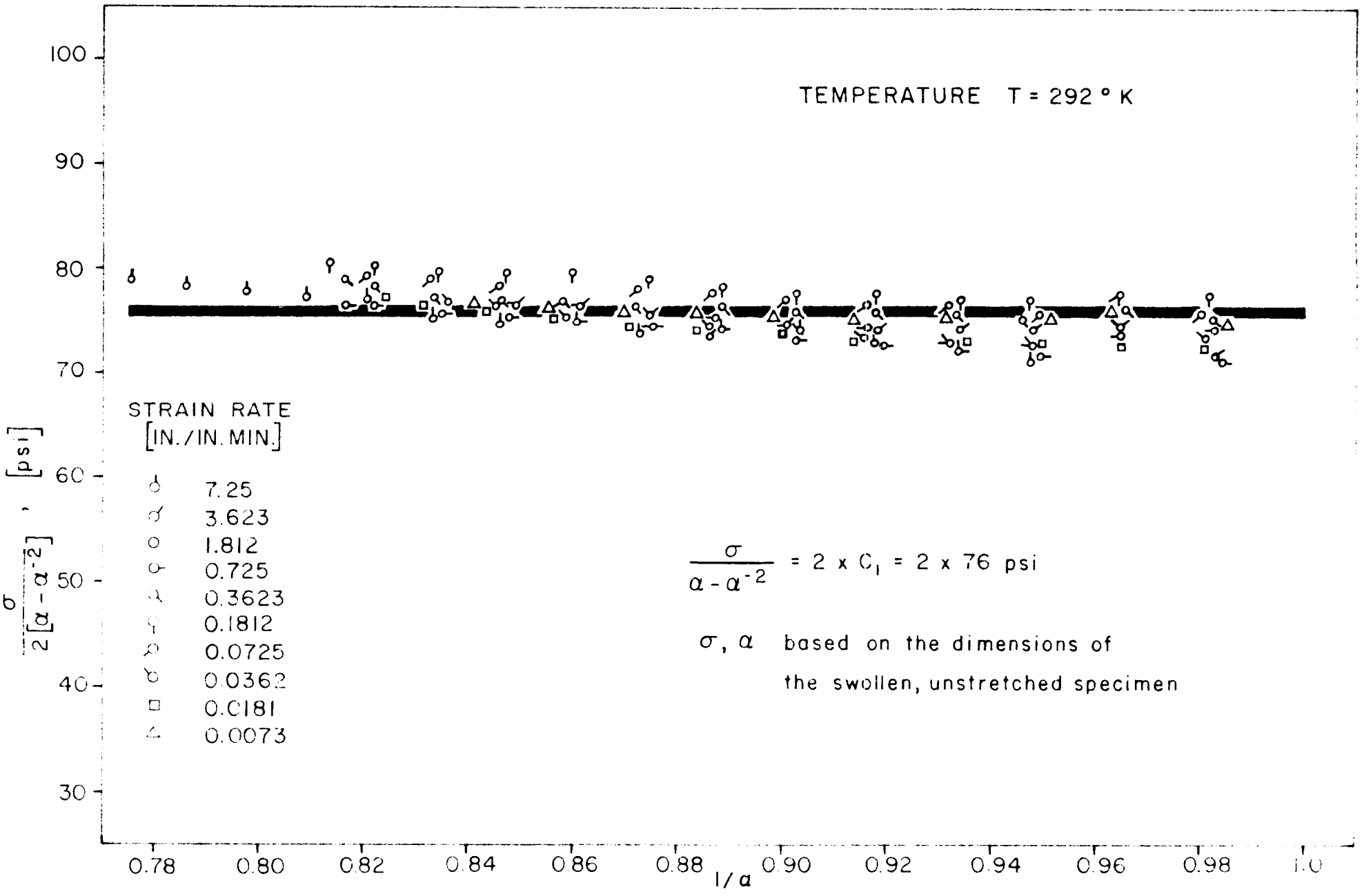

FIG.6 MOONEY-RIVLIN PLOT FOR SOLITHANE 50/50 SWOLLEN IN TOLUENE

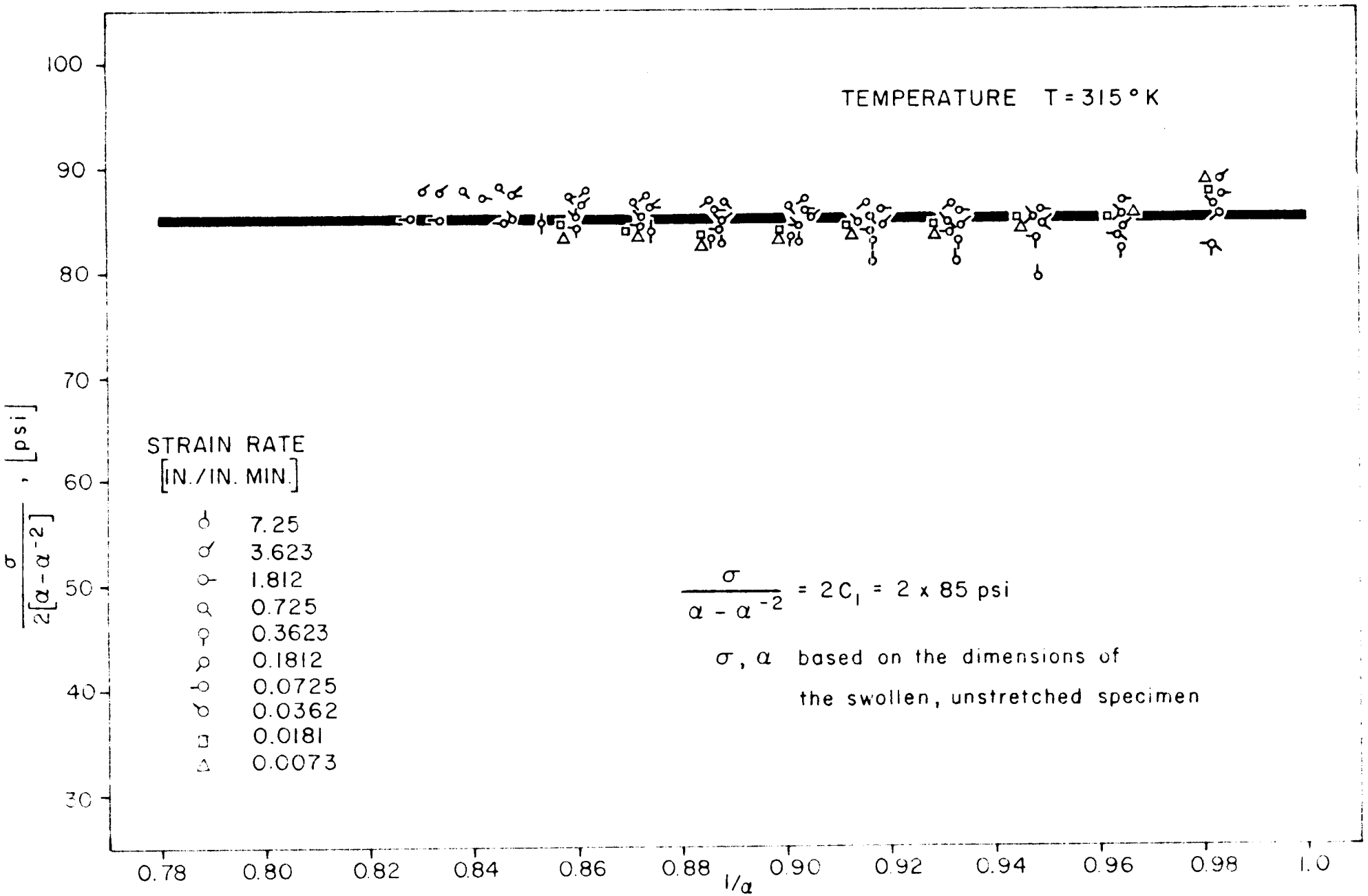

FIG. 7 MOONEY-RIVLIN PLOT FOR SOLITHANE 50/50 SWOLLEN IN TOLUENE

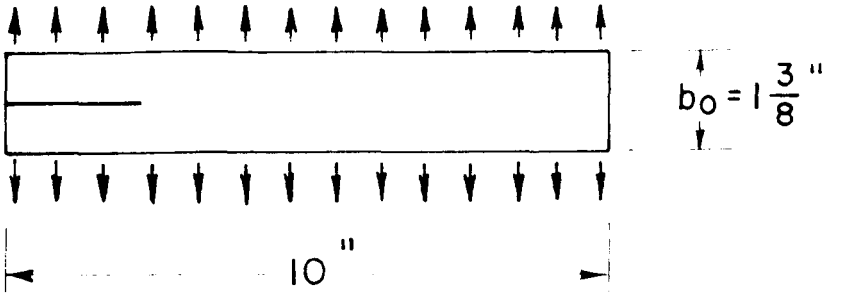

(a) Undeformed geometry of dental dam rubber sheet (0.010 thick)

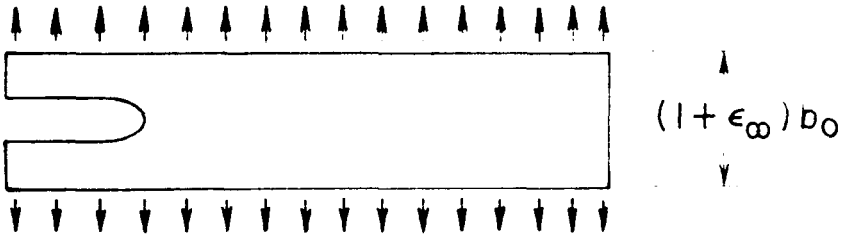

(b) Deformed geometry (ϵ_∞ = gross strain)
(deformation shown corresponds to $\epsilon_\infty \cong 0.4$ at which value first tearing was observed)

FIG. 8 EXPERIMENTAL GEOMETRY

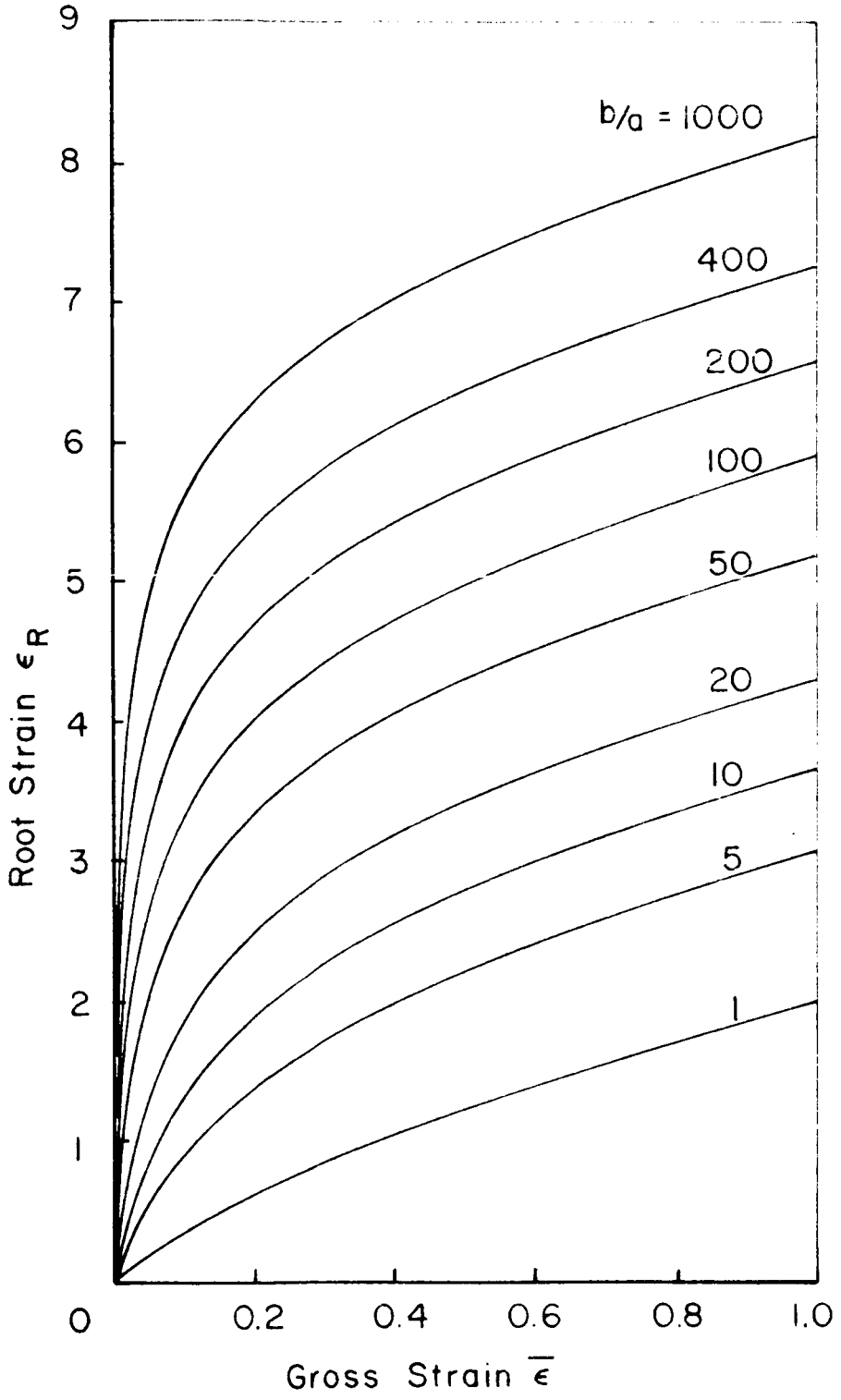

FIG. 9 ROOT STRAIN IN AN ELLIPTICALLY PERFORATED SHEET AS A FUNCTION OF GROSS STRAIN (GEOMETRY, SEE FIG. 8)

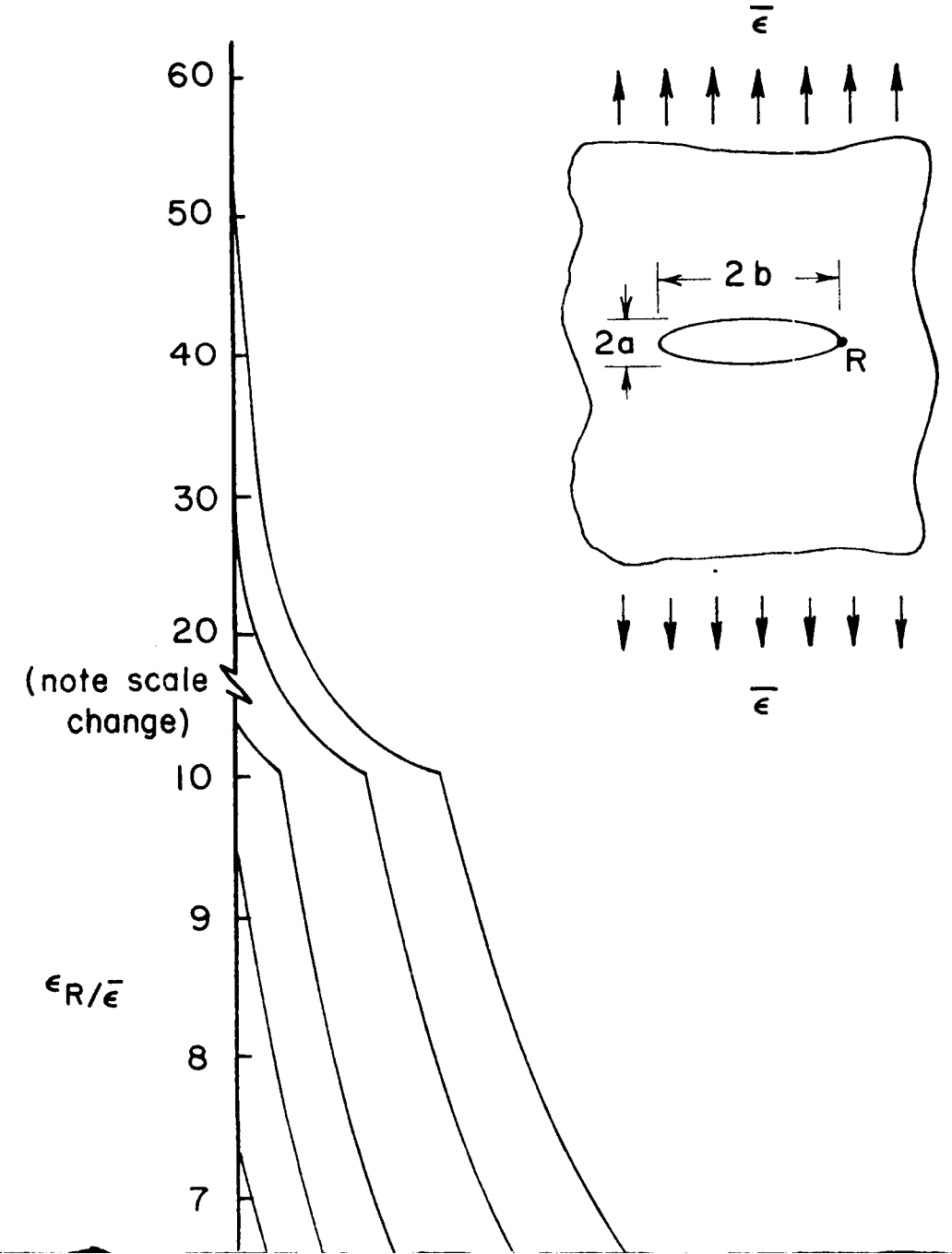
60
50
40
30
20
(note scale change)
10
9
8
7
$\epsilon_R/\bar{\epsilon}$
$\bar{\epsilon}$
2b
2a
R
$\bar{\epsilon}$

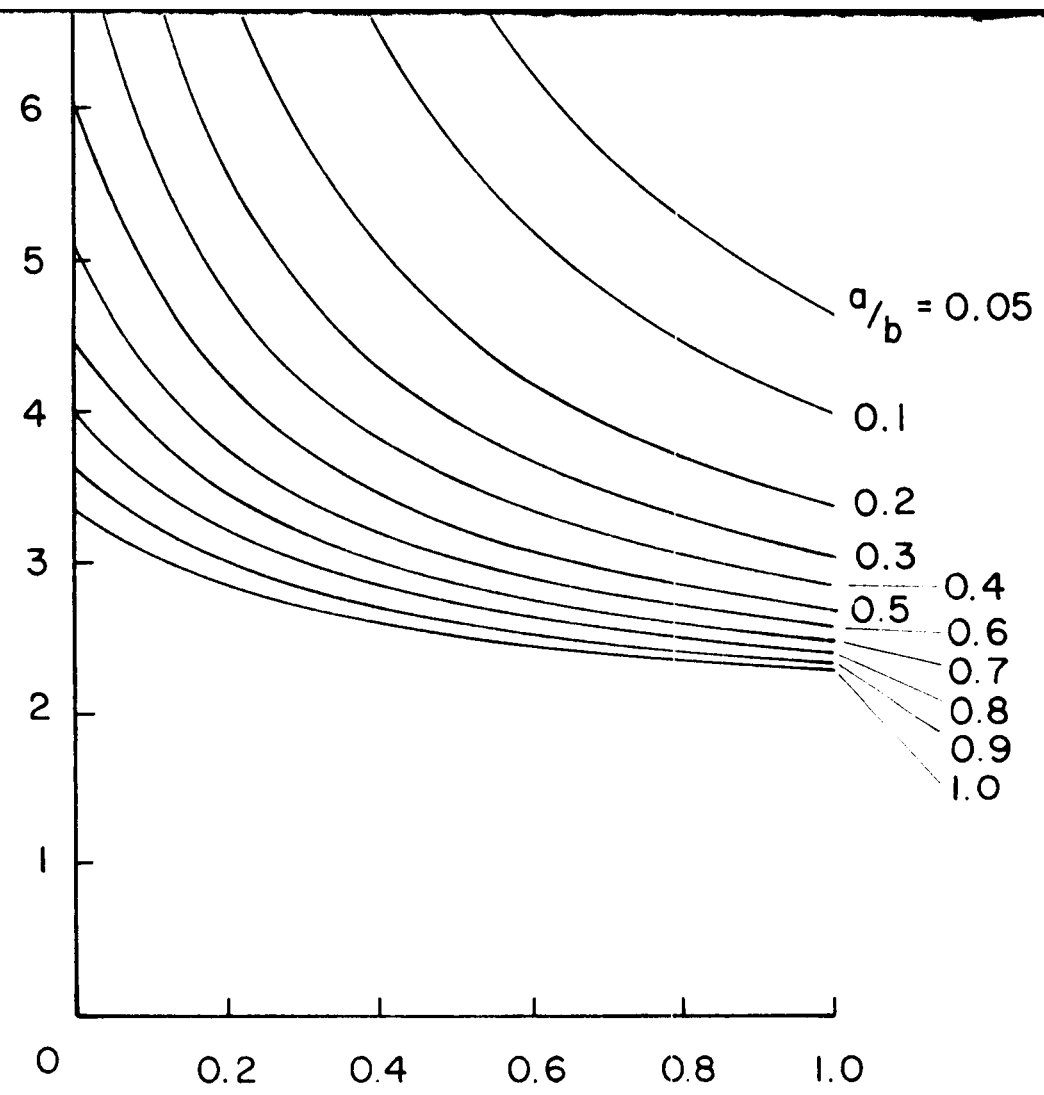

FIG. 10 MAXIMUM STRAIN CONCENTRATION FACTOR IN ELLIPTICALLY PERFORATED SHEET UNDER GROSS STRAIN $\bar{\epsilon}$

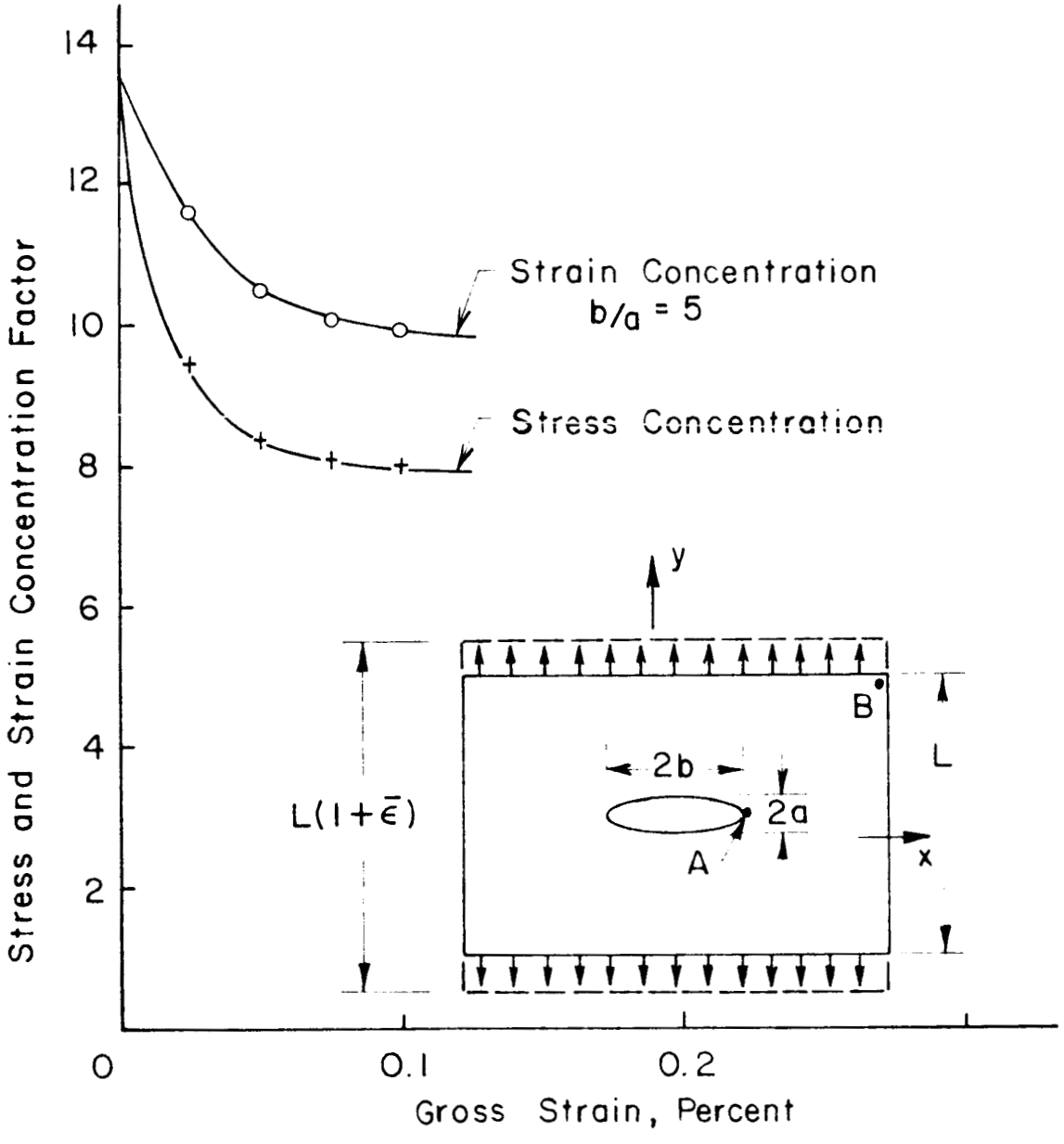

FIG. 11 STRESS CONCENTRATION FACTOR (σ_{yA}/σ_{yB}) AND STRAIN CONCENTRATION FACTOR ($\epsilon_{yA}/\bar{\epsilon}$) AS A FUNCTION OF GROSS STRAIN $\bar{\epsilon}$, FOR NEO-HOOKEAN MATERIAL

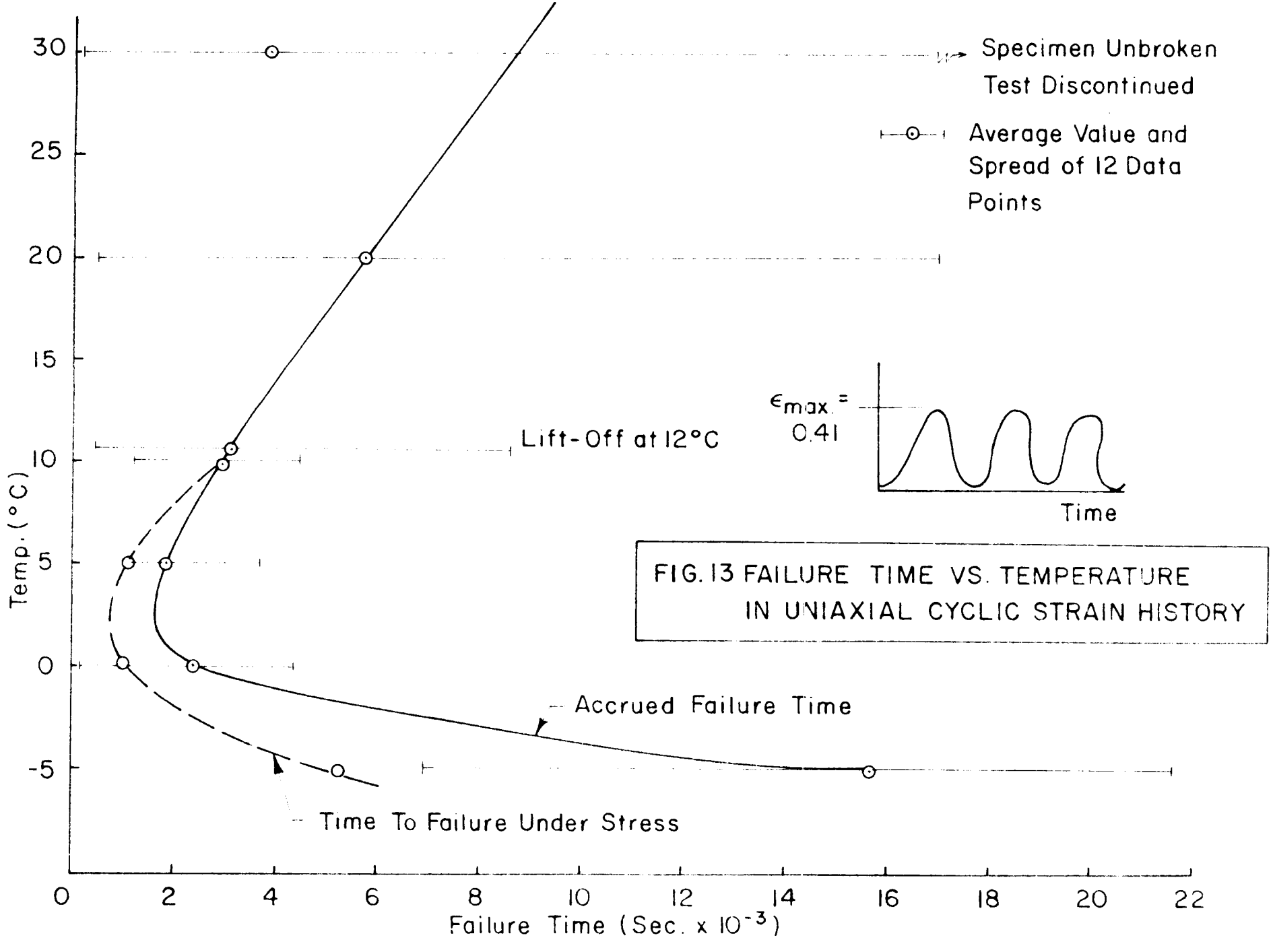

FIG. 13 FAILURE TIME VS. TEMPERATURE IN UNIAXIAL CYCLIC STRAIN HISTORY

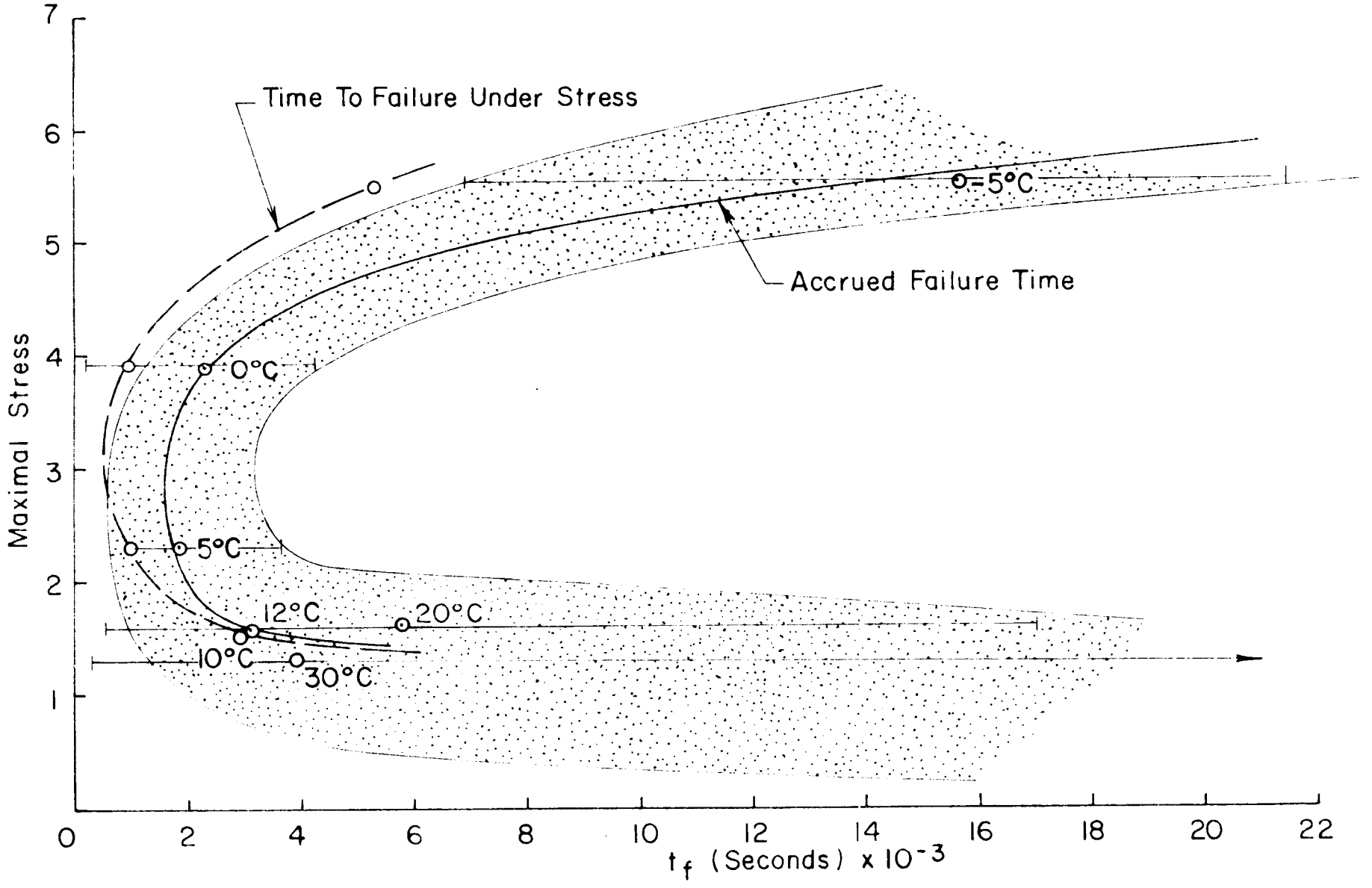

FIG. 14 FAILURE TIME IN UNIAXIAL CYCLIC STRAIN HISTORY VS. MAXIMUM CYCLE STRESS

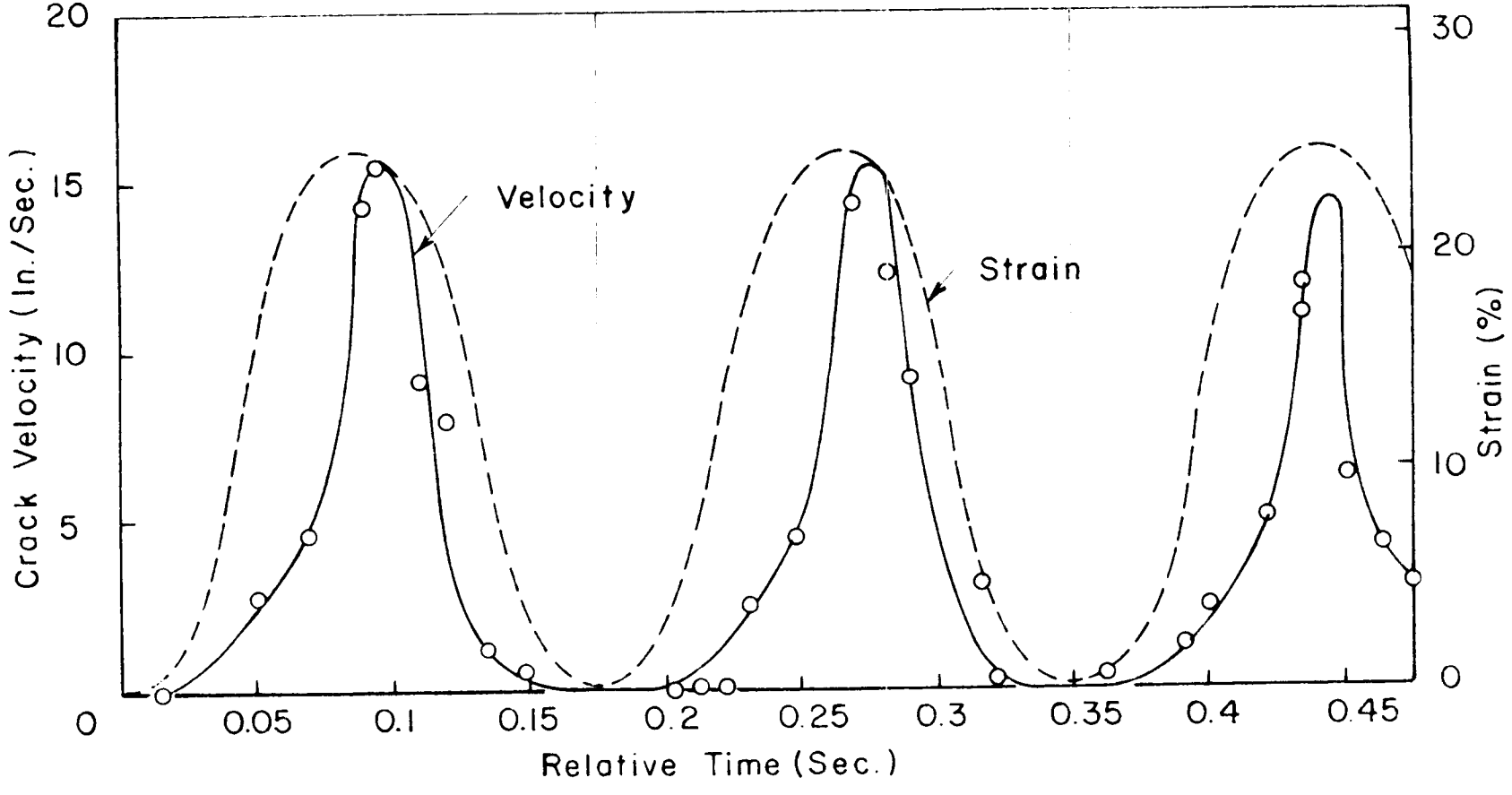

FIG. 15 STRAIN AND CRACK VELOCITY AS A FUNCTION OF TIME